NANO LETTERS

pubs.acs.org/NanoLett Letter

Shear Strain-Induced Two-Dimensional Slip Avalanches in Rhombohedral MoS_2

Jing Liang, Dongyang Yang, Yunhuan Xiao, Sean Chen, Jerry I. Dadap, Joerg Rottler, and Ziliang Ye*

Cite This: *Nano Lett.* 2023, 23, 7228−7235 Read Online

ACCESS | Metrics & More | Article Recommendations | Supporting Information

ABSTRACT: Slip avalanches are ubiquitous phenomena occurring in three-dimensional materials under shear strain, and their study contributes immensely to our understanding of plastic deformation, fragmentation, and earthquakes. So far, little is known about the role of shear strain in two-dimensional (2D) materials. Here we show some evidence of 2D slip avalanches in exfoliated rhombohedral MoS_2, triggered by shear strain near the threshold level. Utilizing interfacial polarization in 3R-MoS_2, we directly probe the stacking order in multilayer flakes and discover a wide variety of polarization domains with sizes following a power-law distribution. These findings suggest that slip avalanches can occur during the exfoliation of 2D materials, and the stacking orders can be changed via shear strain. Our observation has far-reaching implications for the development of new materials and technologies, where precise control over the atomic structure of these materials is essential for optimizing their properties as well as for our understanding of fundamental physical phenomena.

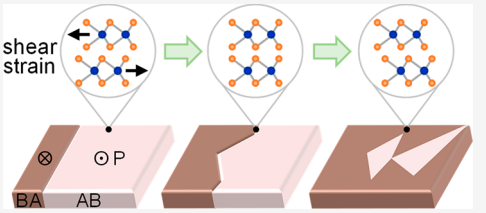

KEYWORDS: *2D materials, slip avalanche, ferroelectricity, shear strain, mechanical exfoliation*

Power-law distributions are a common occurrence in nature and can provide significant insights into various phenomena.[1−4] In material systems, one well-known example of the power-law distribution is the critical behavior that occurs near a phase transition. Even when materials have different compositions and structures, they will share the same critical power-law exponent if they are part of the same universality class.[5] Beyond the phase transition at the thermal equilibrium limit, power-law distributions and universality classes can also be found in non-equilibrium transitions,[6] which often involve external driving forces. For example, when solids are stressed above a critical level, a cascade of strain drops can occur through isolated slip events, known as the slip avalanche phenomenon.[7−21] The size of these slips follows a power-law distribution in a wide range of three-dimensional solids ranging from nanocrystals to earthquakes, spanning more than 12 orders of magnitude of the length scale.[19]

Two-dimensional (2D) materials have provided a unique platform for studying new science and technology at the atomic level. These materials, which are exfoliated from van der Waals (vdW) crystals, have a bonding force between atomic layers much weaker than the intralayer bond. As a result, out-of-plane compressive strain is widely used to tune the interlayer distance and coupling in these materials.[22−24] In contrast, in-plane shear strain can also be generated between layers in 2D materials, but its effect has not been previously investigated. In this study, we report the discovery of a power-law distribution of the polarization domain size in exfoliated molybdenum disulfide (MoS_2) with a rhombohedral stacking order. We attribute this highly abnormal domain size distribution among polarization domains to an interlayer slip avalanche induced by a shear strain near the threshold. Our findings suggest that slip avalanches can occur in 2D materials at the mechanical exfoliation stage, highlighting the potential for exploring the interlayer coupling of 2D materials in new ways.

2D materials with rhombohedral stacking order exhibit a range of fascinating emergent properties. For instance, in rhombohedral trilayer graphene, unconventional superconductivity has been observed in proximity to a metallic phase with reduced isospin symmetry.[25,26] Similarly, rhombohedral transition metal dichalcogenides (TMDs) exhibit asymmetric interlayer coupling, resulting in spontaneous out-of-plane polarization[27] that can be switched by an external electric field via in-plane sliding.[28] This unique property makes them attractive for a range of optoelectronic applications.[29−32] However, fully understanding the detailed stacking order in flakes of atomic thickness is a nontrivial task. As an example, in artificially stacked TMDs with marginal twists, the atomic lattice can naturally relax into a periodic array of nanoscale domains with alternating stacking orders.[33−35] To address such a challenge, we use electrical force microscopy (EFM) and Kelvin probe force microscopy (KPFM) to investigate the

Received: April 20, 2023
Revised: June 21, 2023
Published: June 26, 2023

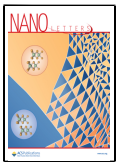

https://doi.org/10.1021/acs.nanolett.3c01487
Nano Lett. 2023, 23, 7228−7235

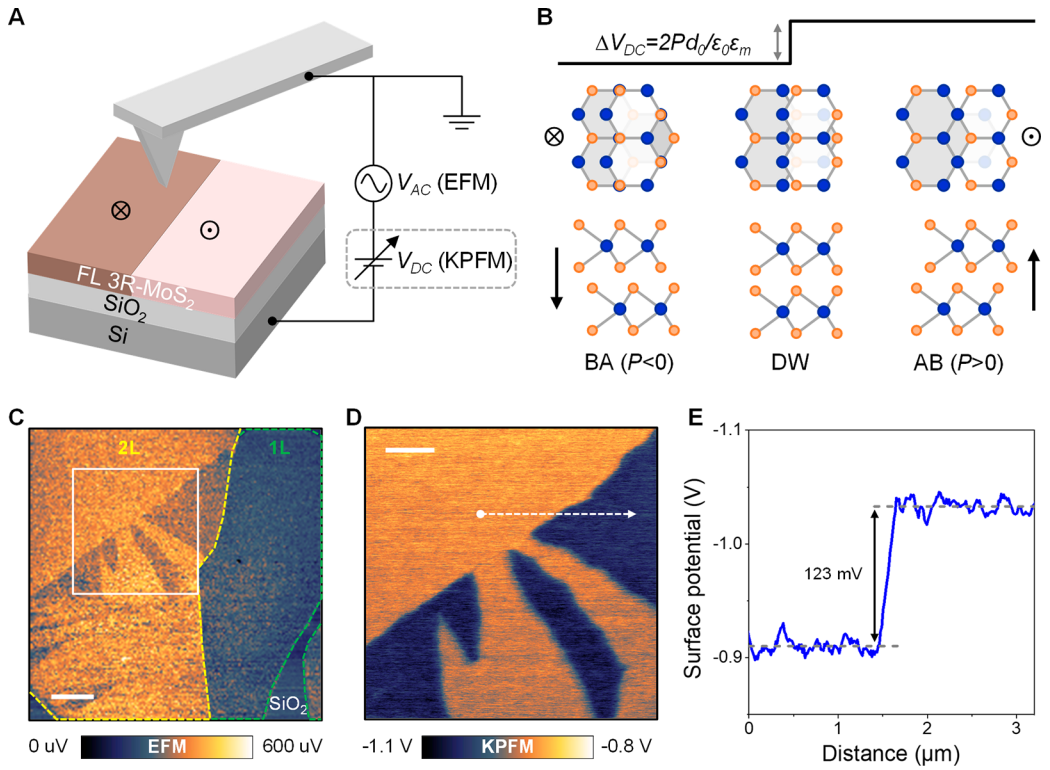

Figure 1. Visualizing stacking configurations in 3R-MoS_2. (A) Illustration of the experimental setup and the sample geometry. Kelvin probe force microscopy (KPFM) measures local surface potential V_{DC} with a DC voltage as feedback. Electrostatic force microscopy (EFM) measures the electrostatic force between the tip and sample surface. (B) Top view (top row) and side view (bottom row) illustration of a 3R-MoS_2 bilayer with BA (P < 0), saddle point (domain wall), and AB (P > 0) stacking configurations. The blue and orange circles denote the Mo and S atoms, respectively. For the sake of clarity, the bottom layer is shaded in gray. The corresponding polarization directions are marked by black arrows. (C) EFM mapping of a 3R-MoS_2 flake with both mono- and bilayer regions. Scale bar, 2 μm. (D) Surface potential mapping of the 3R-MoS_2 bilayer region enclosed by the white box in panel C. Scale bar, 1 μm. (E) Surface potential contrast measured along the dashed line in panel D, which is commensurate with the interlayer potential.

spontaneous polarization in rhombohedral MoS_2 flakes exfoliated from chemically synthesized 3R crystals.[36,37]

EFM and KPFM are powerful techniques for characterizing polar materials with high spatial resolution.[38] The principle of applying them to probe the stacking configuration in 3R-MoS_2 is illustrated in panels A and B of Figure 1. With bilayer 3R-MoS_2 as an example, two symmetric stacking configurations can coexist within a flake. AB stacking denotes the stacking configuration in which the sulfur atom in the top layer lies above the molybdenum atom in the bottom layer, while BA stacking is the mirror image of the AB stacking configuration. Between the two stacking domains is a narrow domain wall region where one layer of MoS_2 is strained (Figure S1).[39] In the AB stacking, because the spontaneous polarization has been determined to be upward,[27] the resultant downward depolarization electric field leads to a higher surface potential. In the BA stacking, the polarization and depolarization fields are reversed, giving rise to a lower surface potential (Figure 1B). Assuming the SiO_2 layer is sufficiently thin so the bottom layer in the entire flake has the same electric potential as the substrate,[40] we find the total difference in surface potential V_{DC} between the two domains is twice the interlayer potential, $\Delta V_{DC} = 2Pd_0/\varepsilon_0\varepsilon_m$, where P is the polarization strength, d_0 and ε_m are the thickness and dielectric constant of monolayer MoS_2, respectively, and ε_0 is the free-space permittivity. As the surface potential can induce an electrostatic force on an adjacent atomic force microscope (AFM) probe, the surface potential contrast between the two types of domains can be visualized in the EFM mode. If a feedback voltage V_{DC} is supplied to compensate for the potential difference between the surface and tip, ΔV_{DC} can be quantitatively measured in the KPFM mode. In our experiment, the voltage is applied between the AFM tip and the highly conductive Si substrate (Figure 1A and Methods in the Supporting Information). Because the capacitance between the tip and sample is orders of magnitude smaller than that between the sample and substrate, the voltage drop across the SiO_2 is negligible (Supporting Text S1).

We first apply these two imaging techniques to a flake consisting of monolayer and bilayer regions (Figure 1C). After EFM mapping was performed, two types of domains with a clear electrostatic force contrast show up in the bilayer region, in stark contrast to the homogeneous monolayer region. In the meantime, no corresponding contrast exists in the topography, indicating the signal originates purely from the stacking-induced surface potential difference (Figure S3). Compared to the artificial stack, the domains in 3R-MoS_2 do not usually have obvious periodicity and often have much larger sizes. To quantify ΔV_{DC}, we focused on a domain wall area and carried out the KPFM measurements (Figure 1D). The surface potential profile across the domain wall indicates a potential difference of 123 $\pm$ 12 meV, consistent with previous experimental reports.[27,35] We have also performed EFM and KPFM measurements in a 2H-MoS_2 flake with different thicknesses as a control (Figure S4), and they show little surface potential contrast. These findings confirm that the

https://doi.org/10.1021/acs.nanolett.3c01487
Nano Lett. 2023, 23, 7228−7235

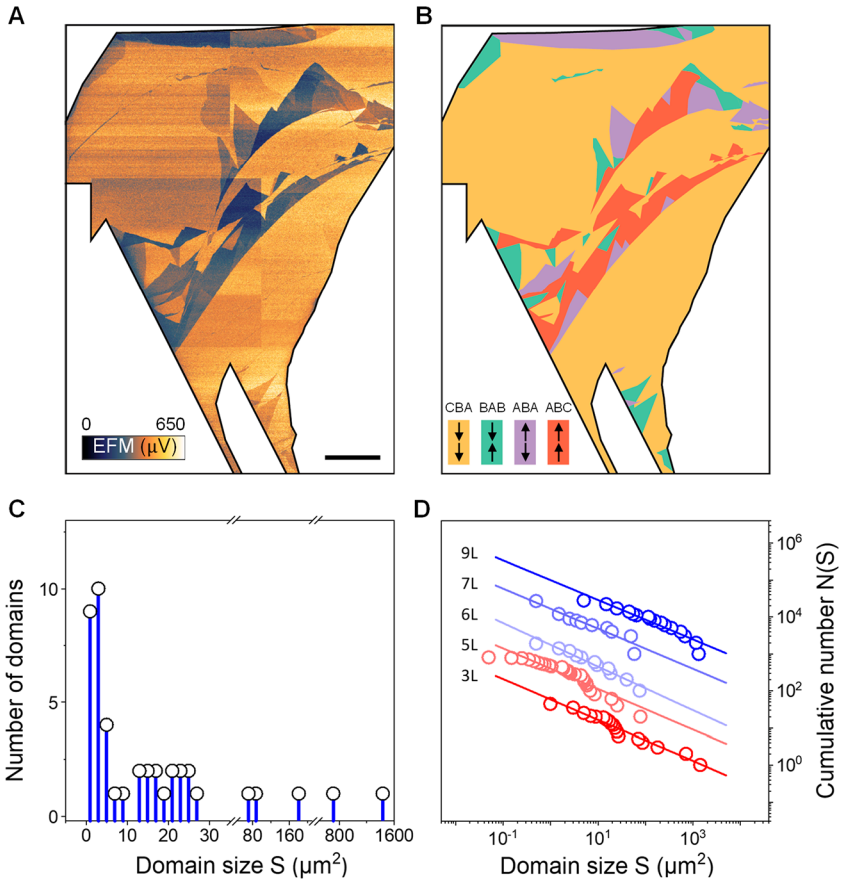

Figure 2. Domain size distribution of a 3R-MoS_2 trilayer. (A) EFM mapping of a 3R-MoS_2 trilayer. Scale bar, 10 μm. (B) Corresponding stacking configuration map of panel A. The colors yellow, green, purple, and red color represent four stacking configurations in trilayers as determined by the surface potential contrast: CBA, BAB, ABA, and ABC, respectively. (C) Histogram of the domain size, regardless of the specific stacking order. (D) Cumulative number $N(S)$ of domains with a size larger than S vs domain size S of five different samples with varying thicknesses. The solid line fit suggests the data follow a power-law dependence. To offset the data, the cumulative numbers of 5L, 6L, 7L, and 9L samples are multiplied by 20, 100, 1000, and 1000, respectively, for the sake of clarity. The fitted power-law exponents κ are summarized in Table S1.

contrast observed in the EFM and KPFM images originates from the rhombohedral stacking configuration.

Compared with the bilayer case, the surface potential map of thicker 3R-MoS_2 flakes exhibits some interesting differences. First, the surface potential contrast across the domain wall is no longer single-valued. In a trilayer flake, four kinds of distinguishable surface potentials are observed in the EFM map (Figure 2A). (Some contrast is a stitching artifact as a single scan cannot cover the entire flake as shown in the topography image (Fig. S5). A homogeneous optical image of the flake is also shown in Figure S5.) This result is interesting, as a trilayer has two interfaces, which can afford four possible stacking configurations [CBA (↓, ↓), BAB (↓, ↑), ABA (↑, ↓), and ABC (↑, ↑), with arrows indicating the polarization direction at each interface]. The CB and BC stacking are equivalent to the BA and AB stacking, respectively. Among the four stacking configurations, BAB and ABA should give the same surface potential because the polarizations from adjacent interfaces are antiparallel to each other. However, the four observed surface potential levels suggest that the degeneracy between the ABA and BAB configurations is broken. Such a broken degeneracy in the surface potential among symmetric configurations is robust in experiments, as even more ΔV_{DC} values are observed in flakes thicker than the trilayer (an eight-layer result and analysis is shown in Figures S6 and S7).

After comparing our observations with previous KPFM studies in few-layer graphene,[41,42] we conclude that the broken degeneracy can be explained by the substrate doping effect. As the SiO_2 substrate inevitably dopes electrons in the MoS_2 flake, free carriers tend to reside in the layer of the lowest potential, which is different between the BAB and ABA stacking configurations. As a result, the electric field between layers becomes modified, which ultimately changes the surface potential relative to the substrate. In Supporting Text S2, we have built a discrete Thomas−Fermi model to discuss such broken degeneracy in detail. According to this model, we color-code the EFM domains by their corresponding stacking configuration. Several domains with curved boundaries are discarded as they are unlikely intrinsic to the stacking configuration.

The second interesting aspect of the trilayer EFM map concerns the size of the polarization domain and its distribution. As shown in Figure 2B, two very large CBA yellow domains occupy >90% of the flake, and many small domains occupy the rest. In total, there are nearly 40 domains within this 40 μm × 40 μm flake. More than 30 domains are <5 μm^2 in size, while a few others are orders of magnitude larger (Figure 2C). Overall, these domains form a highly abnormal size distribution, which we do not expect to originate from the crystal growth, because a crystal grown from a single seed should not have such a high density of stacking faults[29,36]

https://doi.org/10.1021/acs.nanolett.3c01487
Nano Lett. 2023, 23, 7228−7235

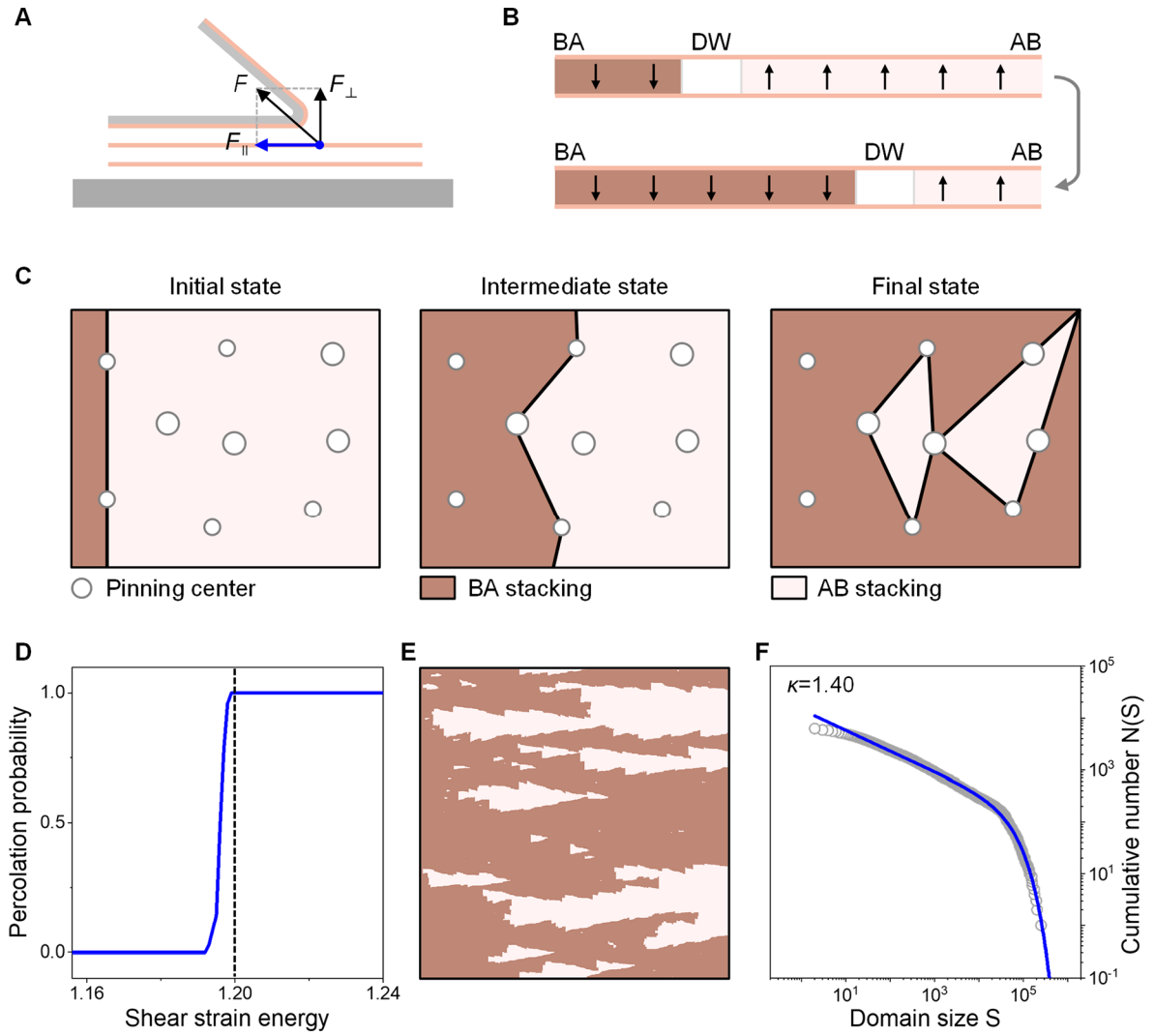

Figure 3. Shear force-induced two-dimensional slip avalanches. (A) Schematic of the mechanical exfoliation process. Gray and orange parts are the exfoliation handle and MoS_2 layers. F is the total force applied to the crystal surface. $F_\perp$ and $F_\parallel$ are the normal and shear force components, respectively. (B) Under a shear strain, the stacking order can be switched, which is equivalent to a domain wall (DW) moving rightward. The brown and pink regions represent the BA and AB domains, respectively, while the arrow indicates the polarization direction. (C) Illustration of the slip avalanche process. When the shear strain energy is larger than the pinning potential, the domain wall becomes depinned until it is trapped by another pinning center with an even stronger pinning potential. A 2D network of strong pinning centers can keep some AB domains from being flipped. (D) Simulated probability for the BA domain to percolate the entire simulation space (900 × 900) under different shear strain energies. The dashed line denotes the critical shear strain energy for the depinning transition. (E) Representative simulation result corresponding to the shear strain energy under the dashed line condition, ~1.201. (F) Statistics of the simulated domain size under the same critical condition. The fit is based on the power-law dependence in addition to the exponential cutoff due to the limited simulation space.

while a crystal grown out of multiple seeds should have a Gaussian distribution in domain size.[43,44]

The distribution of the domain size becomes clear when the cumulative number of domains below a certain domain size, S, $N(S)$, is plotted versus S in a log–log plot. The cumulative plot is often used when the total sample number is not sufficient to directly perform statistics on the probability distribution.[45] In our experiments, tens of domains can be directly observed in a single homogeneous flake. (Among multiple batches of samples, ~20% of the flakes exhibit such high domain densities.) As shown in Figure 2D, a linear fit can match all data points spanning 4 orders of magnitude in size, suggesting the cumulative domain number is approximately a power-law function of domain size: $N(S) \sim S^{-(\kappa-1)}$. In other words, the probability for a domain of a certain size to appear is also power-dependent on the domain size with an exponent κ of ~1.55 according to our fit (Table S1 and Methods in the Supporting Information). Similar power-law distributions are observed in multiple flakes of different thicknesses (Figure S8). Although the detailed stacking configuration can no longer be individually assigned among thicker flakes, the parallel fit lines in the cumulative plot indicate that different samples share a similar power-law exponent (Table S1).

As introduced in the beginning, the slip avalanches observed in a wide range of solid-state systems have a universal power-law exponent of ~1.5,[19] which is close to our fitted κ. We therefore interpret the experimental observation as evidence of a two-dimensional slip avalanche during the mechanical exfoliation process triggered by an in-plane shear force (Figure 3A). Mechanical exfoliation has been an indispensable approach for preparing high-quality 2D materials. During exfoliation, an external force is imposed on the material surface

https://doi.org/10.1021/acs.nanolett.3c01487
Nano Lett. 2023, 23, 7228−7235

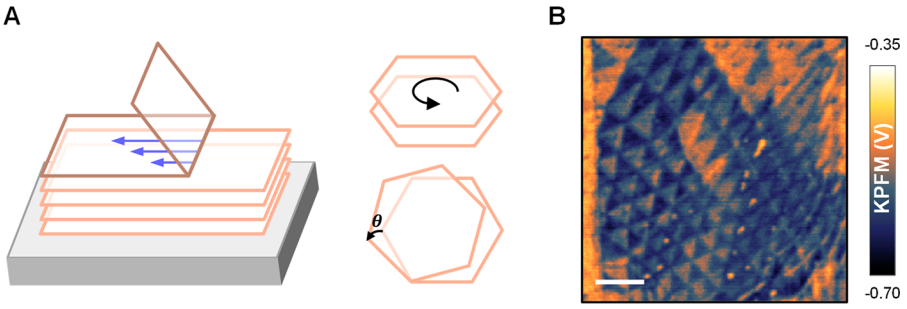

Figure 4. Inhomogeneous shear force-induced interlayer rotation. (A) An inhomogeneous shear force applied to the 3R-MoS_2 surface can induce an interlayer twist. (B) KPFM mapping of a twisted 3R-MoS_2 flake induced by inhomogeneous shear force during the exfoliation. Scale bar, 400 nm.

mostly along surface normal direction $F_\perp$ using some adhesive handle. If $F_\perp$ overcomes the vdW bonding force between layers, then delamination happens, which stochastically leaves atomically thin flakes on the substrate. On the other hand, the exfoliation force unavoidably has in-plane components in practice ($F_\parallel$).[46,47] Because the bottom of the remaining flake is attached to the substrate, $F_\parallel$ induces a shear strain, which can lead to slip avalanches, as observed in other three-dimensional systems.[19]

Here we model the slip avalanche in 3R-MoS_2 as a cascade of domain wall movements that alter the stacking configuration. For the sake of simplicity, we consider only the tensile domain wall in a bilayer 3R-MoS_2 in which the domain wall lattice undergoes a tensile strain and the interlayer displacement direction is perpendicular to the domain wall (Figure 3B and Figure S1A).[39] Given the weak vdW bonding between two layers, an in-plane shear force can move the top layer leftward, converting the AB domain near the domain wall to BA stacking.[48] Effectively, the domain wall moves rightward, antiparallel to the shear force direction. The domain wall of the shear type, where the interlayer displacement direction is parallel to the domain wall, is expected to move perpendicular to the force direction with similar characteristics (Figure 3B and Figure S1B).

A real 2D crystal is not perfect; an exfoliated flake can host a network of quenched disorders, which can hinder the domain wall movement, commonly known as pinning centers. These pinning centers can be atomic defects or localized residual strain. When the domain wall is pinned, a shear force overcoming the pinning potential can depin the domain wall and let it sweep through a portion of the flake until becoming pinned again by a stronger pinning center (Figure 3C). Collectively, a 2D network of randomly distributed pinning centers with varying potential strengths can lead to a critical shear force threshold for the domain wall to sweep throughout the entire flake, according to the non-equilibrium depinning transition theory.[49,50] Right above the critical threshold, we expect that some isolated domains are protected by strong pinning centers and remain unslipped, giving rise to a power-law distribution of domain sizes.

In light of this picture, we adopted a two-dimensional random field Ising model (RFIM) on a square lattice to simulate qualitatively the shear force-induced domain wall movement.[49−52] Before the avalanche happens, the entire simulation domain has the AB stacking order, except for the leftmost column, as represented by the local polarization state $s = -1$ and $+1$, respectively. Every cell has a local slip threshold energy, $E_i = J\sum_j s_i s_j + p_i$, where s_j is the polarization of the nearest neighbor of the cell s_i, J is the interaction energy between them, and p_i is the local pinning potential. When a global external field is turned on, the E_i of every cell is computed to determine whether shear strain energy ε is larger than the local threshold energy. The polarization of a cell is switched from -1 to $+1$ if the slipping criterion is met. The external field scanning is carried out column by column, left to right, to mimic the domain wall propagation effect. When the BA domain reaches the rightmost column, a domain wall percolation is achieved by the external field. More details about the RFIM simulation can be found in Supporting Text S3.

We first find the critical external field by simulating the RFIM model 100 times, each time with a randomly generated pinning potential network (Figure 3D). When the ratio of shear strain energy to interaction energy is >1.2, the domain wall can sweep through the simulation space with a percolation probability of ∼1. The critical field is found to be insensitive to the simulation space size or detailed pinning potential distribution (Figure S9A). Seven representative simulation results under different values of shear force are shown in Figure 3E and Figure S10. As predicted by the depinning transition theory, the domain wall either is stuck by pinning centers under weak shear forces (Figure S10A−C) or sweeps through the whole space under strong shear forces (Figure S10D−F). Only near the critical point (Figure 3E) do the domains in the simulation show shapes similar to those in our experiments. More importantly, the statistics of the domain size under this condition also exhibit a power-law distribution with an exponent close to our experiments, as discussed below. The reason why multiple flakes exfoliated in different batches all experience similar slip avalanches near the critical point in our experiments might be biased by statistics; those that are away from the critical point exhibit little domain contrast and therefore cannot provide sufficient statistics on the domain size.

Next, we perform a statistical analysis on the simulated domains in the vicinity of the critical point. Because all slipped units are connected as a single percolated domain, the isolated unslipped domains account for the majority of the statistics. As shown in Figure 3F, the domain size distribution follows a power law with an exponent of ∼1.40, comparable to our experimental findings. The deviation from the power-law distribution in the large and small domain limit is known to be caused by the size of the simulation space and the spatial resolution, respectively.[19,53] Similar to the critical field, the exponent is not very sensitive to the simulation details (Figure S9B). In future studies, other factors such as a triangle lattice and associated anisotropy can be incorporated into a more

https://doi.org/10.1021/acs.nanolett.3c01487
Nano Lett. 2023, 23, 7228−7235

comprehensive model. The fact that the ABC and CBA domains occur more frequently than the ABA and BAB domains in our experiment may suggest certain stacking configurations are more energetically favorable than others.

The shear force-induced interlayer sliding is further evidenced by the large-scale moiré superlattice occasionally observed in exfoliated 3R-MoS_2. As the shear force is unavoidably inhomogeneous during exfoliation, the non-zero moment of the force can lead to a torque and therefore an interlayer rotation (Figure 4A). Similar to that in twisted bilayer graphene, the rotational misalignment between layers gives rise to a moiré superlattice whose period λ depends on twist angle θ, $\lambda = \frac{a}{2\sin(\theta/2)}$, where a is the in-plane lattice constant of monolayer MoS_2 (Figure 4A). If the twist angle is small, the energetically favorable AB and BA stacking domains are maximized through local lattice reconstruction, giving rise to staggered triangle stacking domains.[54,55] Experimentally, we can image these reconstructed domains using KPFM (Figure 4B and Figure S11). In our natural moiré superlattice, the observed period is ∼200 nm, indicating that the twisted angle is ∼0.09°, much smaller than the intentionally created twists in artificial stacks. Such a large period and a correspondingly small twist are also observed in another thick flake with a rich domain contrast (Figure S12).

In this study, we investigated the stacking order of exfoliated few-layer 3R-MoS_2 flakes by utilizing stacking-induced surface potential contrast. We have discovered a variety of polarization domains with a power-law distribution in size, which we attribute to shear strain-induced two-dimensional slip avalanches at the mechanical exfoliation stage. Our findings suggest that shear strain is a promising way to tune the stacking order in TMDs, providing an opportunity to observe non-equilibrium statistical phenomena in two dimensions. Furthermore, it would be intriguing to explore whether slip avalanches can also occur in other 2D materials, such as graphene, because the percentage of rhombohedral domains in exfoliated few-layer graphene is similar to that in bulk graphite,[56] and local strain has been shown to be capable of altering the stacking order of multilayer graphene.[57] Our study provides valuable insights into the fundamental understanding of the properties of 2D materials with a rhombohedral stacking order and opens up new avenues for the design and application of these materials in various fields.

■ ASSOCIATED CONTENT

Supporting Information

The Supporting Information is available free of charge at https://pubs.acs.org/doi/10.1021/acs.nanolett.3c01487.

Descriptions of sample preparation and characterization, circuit model of surface potential measurement, discrete Thomas−Fermi model, two-dimensional random field Ising model, Figures S1−12, and Table S1 (PDF)

■ AUTHOR INFORMATION

Corresponding Author

Ziliang Ye − *Department of Physics and Astronomy, The University of British Columbia, Vancouver, BC V6T 1Z1, Canada; Quantum Matter Institute, The University of British Columbia, Vancouver, BC V6T 1Z4, Canada;* orcid.org/0000-0001-8314-6977; Email: zlye@phas.ubc.ca

Authors

Jing Liang − *Department of Physics and Astronomy, The University of British Columbia, Vancouver, BC V6T 1Z1, Canada; Quantum Matter Institute, The University of British Columbia, Vancouver, BC V6T 1Z4, Canada;* orcid.org/0000-0001-6348-2068

Dongyang Yang − *Department of Physics and Astronomy, The University of British Columbia, Vancouver, BC V6T 1Z1, Canada; Quantum Matter Institute, The University of British Columbia, Vancouver, BC V6T 1Z4, Canada*

Yunhuan Xiao − *Department of Physics and Astronomy, The University of British Columbia, Vancouver, BC V6T 1Z1, Canada; Quantum Matter Institute, The University of British Columbia, Vancouver, BC V6T 1Z4, Canada*

Sean Chen − *Department of Physics and Astronomy, The University of British Columbia, Vancouver, BC V6T 1Z1, Canada; Quantum Matter Institute, The University of British Columbia, Vancouver, BC V6T 1Z4, Canada*

Jerry I. Dadap − *Department of Physics and Astronomy, The University of British Columbia, Vancouver, BC V6T 1Z1, Canada; Quantum Matter Institute, The University of British Columbia, Vancouver, BC V6T 1Z4, Canada*

Joerg Rottler − *Department of Physics and Astronomy, The University of British Columbia, Vancouver, BC V6T 1Z1, Canada; Quantum Matter Institute, The University of British Columbia, Vancouver, BC V6T 1Z4, Canada;* orcid.org/0000-0002-5273-7480

Complete contact information is available at: https://pubs.acs.org/10.1021/acs.nanolett.3c01487

Author Contributions

Z.Y. and J.L. conceived the project. J.L., D.Y., and Y.X. prepared the samples. J.L. performed the sample characterization and data analysis. J.L. and S.C. calculated the discrete Thomas−Fermi model under Z.Y.'s supervision. J.L. simulated the 2D RFIM under the supervision of Z.Y. and J.R. J.L., Z.Y., and J.I.D. wrote the paper with input from all authors.

Notes

The authors declare no competing financial interest.

■ ACKNOWLEDGMENTS

This work is supported by the Natural Sciences and Engineering Research Council of Canada, Canada Foundation for Innovation, New Frontiers in Research Fund, Canada First Research Excellence Fund, Quantum Materials and Future Technologies Program, Max Planck−UBC−UTokyo Center for Quantum Materials, and Gordon and Betty Moore Foundation's EPiQS Initiative (GBMF11071). Z.Y. is also supported by the Canada Research Chairs Program.

■ REFERENCES

(1) Adamic, L. A.; Lukose, R. M.; Puniyani, A. R.; Huberman, B. A. Search in power-law networks. *Phys. Rev. E* **2001**, *64*, 046135.

(2) Gabaix, X.; Gopikrishnan, P.; Plerou, V.; Stanley, H. E. A theory of power-law distributions in financial market fluctuations. *Nature* **2003**, *423*, 267−270.

(3) Kilpatrick, A. M.; Ives, A. R. Species interactions can explain Taylor's power law for ecological time series. *Nature* **2003**, *422*, 65−68.

(4) Aharonian, F.; Yang, R.; de Oña Wilhelmi, E. Massive stars as major factories of Galactic cosmic rays. *Nature Astronomy* **2019**, *3*, 561−567.

(5) Sethna, J. P. Power laws in physics. *Nature Reviews Physics* **2022**, *4*, 501−503.
(6) Henkel, M.; Hinrichsen, H.; Lübeck, S. *Non-Equilibrium Phase Transitions*; Springer, 2008.
(7) Carlson, J. M.; Langer, J. S. Properties of earthquakes generated by fault dynamics. *Phys. Rev. Lett.* **1989**, *62*, 2632−2635.
(8) Zapperi, S.; Vespignani, A.; Stanley, H. E. Plasticity and avalanche behaviour in microfracturing phenomena. *Nature* **1997**, *388*, 658−660.
(9) Csikor, F. F.; Motz, C.; Weygand, D.; Zaiser, M.; Zapperi, S. Dislocation Avalanches, Strain Bursts, and the Problem of Plastic Forming at the Micrometer Scale. *Science* **2007**, *318*, 251−254.
(10) Maloney, C. E.; Robbins, M. O. Anisotropic Power Law Strain Correlations in Sheared Amorphous 2D Solids. *Phys. Rev. Lett.* **2009**, *102*, 225502.
(11) Dahmen, K. A.; Ben-Zion, Y.; Uhl, J. T. Micromechanical Model for Deformation in Solids with Universal Predictions for Stress-Strain Curves and Slip Avalanches. *Phys. Rev. Lett.* **2009**, *102*, 175501.
(12) Sun, B. A.; Yu, H. B.; Jiao, W.; Bai, H. Y.; Zhao, D. Q.; Wang, W. H. Plasticity of Ductile Metallic Glasses: A Self-Organized Critical State. *Phys. Rev. Lett.* **2010**, *105*, 035501.
(13) Papanikolaou, S.; Bohn, F.; Sommer, R. L.; Durin, G.; Zapperi, S.; Sethna, J. P. Universality beyond power laws and the average avalanche shape. *Nat. Phys.* **2011**, *7*, 316−320.
(14) Friedman, N.; Jennings, A. T.; Tsekenis, G.; Kim, J.-Y.; Tao, M.; Uhl, J. T.; Greer, J. R.; Dahmen, K. A. Statistics of Dislocation Slip Avalanches in Nanosized Single Crystals Show Tuned Critical Behavior Predicted by a Simple Mean Field Model. *Phys. Rev. Lett.* **2012**, *109*, 095507.
(15) Antonaglia, J.; Wright, W. J.; Gu, X.; Byer, R. R.; Hufnagel, T. C.; LeBlanc, M.; Uhl, J. T.; Dahmen, K. A. Bulk Metallic Glasses Deform via Slip Avalanches. *Phys. Rev. Lett.* **2014**, *112*, 155501.
(16) Antonaglia, J.; Xie, X.; Schwarz, G.; Wraith, M.; Qiao, J.; Zhang, Y.; Liaw, P. K.; Uhl, J. T.; Dahmen, K. A. Tuned Critical Avalanche Scaling in Bulk Metallic Glasses. *Sci. Rep.* **2014**, *4*, 4382.
(17) Ispánovity, P. D.; Laurson, L.; Zaiser, M.; Groma, I.; Zapperi, S.; Alava, M. J. Avalanches in 2D Dislocation Systems: Plastic Yielding Is Not Depinning. *Phys. Rev. Lett.* **2014**, *112*, 235501.
(18) Krisponeit, J.-O.; Pitikaris, S.; Avila, K. E.; Küchemann, S.; Krüger, A.; Samwer, K. Crossover from random three-dimensional avalanches to correlated nano shear bands in metallic glasses. *Nat. Commun.* **2014**, *5*, 3616.
(19) Uhl, J. T.; Pathak, S.; Schorlemmer, D.; Liu, X.; Swindeman, R.; Brinkman, B. A. W.; LeBlanc, M.; Tsekenis, G.; Friedman, N.; Behringer, R.; et al. Universal Quake Statistics: From Compressed Nanocrystals to Earthquakes. *Sci. Rep.* **2015**, *5*, 16493.
(20) Denisov, D. V.; Lörincz, K. A.; Uhl, J. T.; Dahmen, K. A.; Schall, P. Universality of slip avalanches in flowing granular matter. *Nat. Commun.* **2016**, *7*, 10641.
(21) Dahmen, K. A. *Avalanches in Functional Materials and Geophysics*; Springer, 2017; pp 19−30.
(22) Yankowitz, M.; Jung, J.; Laksono, E.; Leconte, N.; Chittari, B. L.; Watanabe, K.; Taniguchi, T.; Adam, S.; Graf, D.; Dean, C. R. Dynamic band-structure tuning of graphene moiré superlattices with pressure. *Nature* **2018**, *557*, 404−408.
(23) Song, T.; Fei, Z.; Yankowitz, M.; Lin, Z.; Jiang, Q.; Hwangbo, K.; Zhang, Q.; Sun, B.; Taniguchi, T.; Watanabe, K.; et al. Switching 2D magnetic states via pressure tuning of layer stacking. *Nat. Mater.* **2019**, *18*, 1298−1302.
(24) Xia, J.; Yan, J.; Wang, Z.; He, Y.; Gong, Y.; Chen, W.; Sum, T. C.; Liu, Z.; Ajayan, P. M.; Shen, Z. Strong coupling and pressure engineering in WSe2−MoSe2 heterobilayers. *Nat. Phys.* **2021**, *17*, 92−98.
(25) Zhou, H.; Xie, T.; Taniguchi, T.; Watanabe, K.; Young, A. F. Superconductivity in rhombohedral trilayer graphene. *Nature* **2021**, *598*, 434−438.
(26) Chatterjee, S.; Wang, T.; Berg, E.; Zaletel, M. P. Inter-valley coherent order and isospin fluctuation mediated superconductivity in rhombohedral trilayer graphene. *Nat. Commun.* **2022**, *13*, 6013.
(27) Liang, J.; Yang, D.; Wu, J.; Dadap, J. I.; Watanabe, K.; Taniguchi, T.; Ye, Z. Optically Probing the Asymmetric Interlayer Coupling in Rhombohedral-Stacked MoS_2 Bilayer. *Physical Review X* **2022**, *12*, 041005.
(28) Mak, K. F.; Lee, C.; Hone, J.; Shan, J.; Heinz, T. F. Atomically Thin MoS_2: A New Direct-Gap Semiconductor. *Phys. Rev. Lett.* **2010**, *105*, 136805.
(29) Fan, X.; Zheng, W. T.; Kuo, J.-L.; Singh, D. J.; Sun, C. Q.; Zhu, W. Modulation of electronic properties from stacking orders and spin-orbit coupling for 3R-type MoS2. *Sci. Rep.* **2016**, *6*, 24140.
(30) Wu, M.; Li, J. Sliding ferroelectricity in 2D van der Waals materials: Related physics and future opportunities. *Proc. Natl. Acad. Sci. U. S. A.* **2021**, *118*, No. e2115703118.
(31) Yang, D.; Wu, J.; Zhou, B. T.; Liang, J.; Ideue, T.; Siu, T.; Awan, K. M.; Watanabe, K.; Taniguchi, T.; Iwasa, Y.; et al. Spontaneous-polarization-induced photovoltaic effect in rhombohedrally stacked MoS_2. *Nat. Photonics* **2022**, *16*, 469−474.
(32) Wu, J.; Yang, D.; Liang, J.; Werner, M.; Ostroumov, E.; Xiao, Y.; Watanabe, K.; Taniguchi, T.; Dadap, J. I.; Jones, D.; et al. Ultrafast response of spontaneous photovoltaic effect in 3R-MoS_2-based heterostructures. *Sci. Adv.* **2022**, *8*, No. eade3759.
(33) Wu, M. Two-Dimensional van der Waals Ferroelectrics: Scientific and Technological Opportunities. *ACS Nano* **2021**, *15*, 9229−9237.
(34) Wang, X.; Yasuda, K.; Zhang, Y.; Liu, S.; Watanabe, K.; Taniguchi, T.; Hone, J.; Fu, L.; Jarillo-Herrero, P. Interfacial ferroelectricity in rhombohedral-stacked bilayer transition metal dichalcogenides. *Nat. Nanotechnol.* **2022**, *17*, 367−371.
(35) Weston, A.; Castanon, E. G.; Enaldiev, V.; Ferreira, F.; Bhattacharjee, S.; Xu, S.; Corte-León, H.; Wu, Z.; Clark, N.; Summerfield, A.; et al. Interfacial ferroelectricity in marginally twisted 2D semiconductors. *Nat. Nanotechnol.* **2022**, *17*, 390−395.
(36) Wildervanck, J. C. Chalcogenides of Molybdenum, Tungsten, Technetium and Rhenium. Ph.D. Thesis, University of Groningen, Groningen, The Netherlands, 1970.
(37) Suzuki, R.; Sakano, M.; Zhang, Y. J.; Akashi, R.; Morikawa, D.; Harasawa, A.; Yaji, K.; Kuroda, K.; Miyamoto, K.; Okuda, T.; et al. Valley-dependent spin polarization in bulk MoS_2 with broken inversion symmetry. *Nat. Nanotechnol.* **2014**, *9*, 611−617.
(38) Deb, S.; Cao, W.; Raab, N.; Watanabe, K.; Taniguchi, T.; Goldstein, M.; Kronik, L.; Urbakh, M.; Hod, O.; Ben Shalom, M. Cumulative polarization in conductive interfacial ferroelectrics. *Nature* **2022**, *612*, 465−469.
(39) Alden, J. S.; Tsen, A. W.; Huang, P. Y.; Hovden, R.; Brown, L.; Park, J.; Muller, D. A.; McEuen, P. L. Strain solitons and topological defects in bilayer graphene. *Proc. Natl. Acad. Sci. U. S. A.* **2013**, *110*, 11256−11260.
(40) Ferreira, F.; Enaldiev, V. V.; Fal'ko, V. I.; Magorrian, S. J. Weak ferroelectric charge transfer in layer-asymmetric bilayers of 2D semiconductors. *Sci. Rep.* **2021**, *11*, 13422.
(41) Datta, S. S.; Strachan, D. R.; Mele, E. J.; Johnson, A. T. C. Surface Potentials and Layer Charge Distributions in Few-Layer Graphene Films. *Nano Lett.* **2009**, *9*, 7−11.
(42) Wang, Z. M. *MoS_2: Materials, Physics, and Devices*, Vol. *6*; Springer, 2014; pp 141−144.
(43) Liu, C.; Xu, X.; Qiu, L.; Wu, M.; Qiao, R.; Wang, L.; Wang, J.; Niu, J.; Liang, J.; Zhou, X.; et al. Kinetic modulation of graphene growth by fluorine through spatially confined decomposition of metal fluorides. *Nat. Chem.* **2019**, *11*, 730−736.
(44) Liu, L.; Li, T.; Ma, L.; Li, W.; Gao, S.; Sun, W.; Dong, R.; Zou, X.; Fan, D.; Shao, L.; et al. Uniform nucleation and epitaxy of bilayer molybdenum disulfide on sapphire. *Nature* **2022**, *605*, 69−75.
(45) Oddershede, L.; Dimon, P.; Bohr, J. Self-organized criticality in fragmenting. *Phys. Rev. Lett.* **1993**, *71*, 3107−3110.

https://doi.org/10.1021/acs.nanolett.3c01487
Nano Lett. 2023, 23, 7228−7235

(46) Yi, M.; Shen, Z. A review on mechanical exfoliation for the scalable production of graphene. *Journal of Materials Chemistry A* **2015**, *3*, 11700−11715.
(47) Liu, F. Mechanical exfoliation of large area 2D materials from vdW crystals. *Prog. Surf. Sci.* **2021**, *96*, 100626.
(48) Nery, J. P.; Calandra, M.; Mauri, F. Long-Range Rhombohedral-Stacked Graphene through Shear. *Nano Lett.* **2020**, *20*, 5017−5023.
(49) Drossel, B.; Dahmen, K. Depinning of a domain wall in the 2d random-field Ising model. *European Physical Journal B - Condensed Matter and Complex Systems* **1998**, *3*, 485−496.
(50) Zapperi, S.; Cizeau, P.; Durin, G.; Stanley, H. E. Dynamics of a ferromagnetic domain wall: Avalanches, depinning transition, and the Barkhausen effect. *Phys. Rev. B* **1998**, *58*, 6353−6366.
(51) Villain, J. Nonequilibrium ″Critical″ Exponents in the Random-Field Ising Model. *Phys. Rev. Lett.* **1984**, *52*, 1543−1546.
(52) Xi, B.; Luo, M.-B.; Vinokur, V. M.; Hu, X. Depinning Transition of a Domain Wall in Ferromagnetic Films. *Sci. Rep.* **2015**, *5*, 14062.
(53) Sethna, J. P.; Dahmen, K. A.; Myers, C. R. Crackling noise. *Nature* **2001**, *410*, 242−250.
(54) Rosenberger, M. R.; Chuang, H.-J.; Phillips, M.; Oleshko, V. P.; McCreary, K. M.; Sivaram, S. V.; Hellberg, C. S.; Jonker, B. T. Twist Angle-Dependent Atomic Reconstruction and Moiré Patterns in Transition Metal Dichalcogenide Heterostructures. *ACS Nano* **2020**, *14*, 4550−4558.
(55) Enaldiev, V. V.; Zólyomi, V.; Yelgel, C.; Magorrian, S. J.; Fal'ko, V. I. Stacking Domains and Dislocation Networks in Marginally Twisted Bilayers of Transition Metal Dichalcogenides. *Phys. Rev. Lett.* **2020**, *124*, 206101.
(56) Lui, C. H.; Li, Z.; Chen, Z.; Klimov, P. V.; Brus, L. E.; Heinz, T. F. Imaging Stacking Order in Few-Layer Graphene. *Nano Lett.* **2011**, *11*, 164−169.
(57) Jiang, L.; Wang, S.; Shi, Z.; Jin, C.; Utama, M. I. B.; Zhao, S.; Shen, Y.-R.; Gao, H.-J.; Zhang, G.; Wang, F. Manipulation of domain-wall solitons in bi- and trilayer graphene. *Nat. Nanotechnol.* **2018**, *13*, 204−208.

https://doi.org/10.1021/acs.nanolett.3c01487
Nano Lett. 2023, 23, 7228−7235